Deep Learning for Posture Control Nonlinear Model System and Noise Identification

Vittorio Lippi[1][a], Thomas Mergner[2][b] and Christoph Maurer[2][c]

[1]*Technical University Berlin, Control Systems, Berlin, Germany*

[2]*Neurological University Clinic, University of Freiburg, Freiburg im Breisgau, Germany*

Keywords: Posture Control, Deep Learning, System Identification, Parametric Nonlinear System.

Abstract: In this work we present a system identification procedure based on Convolutional Neural Networks (CNN) for human posture control models. A usual approach to the study of human posture control consists in the identification of parameters for a control system. In this context, linear models are particularly popular due to the relative simplicity in identifying the required parameters and to analyze the results. Nonlinear models, conversely, are required to predict the real behavior exhibited by human subjects and hence it is desirable to use them in posture control analysis. The use of CNN aims to overcome the heavy computational requirement for the identification of nonlinear models, in order to make the analysis of experimental data less time consuming and, in perspective, to make such analysis feasible in the context of clinical tests. After testing the performance of the CNN on validation and test sets, two examples are presented and discussed from the qualitative point of view: the identification of parameters using data from human experiments and using data of a simulated model with some differences with respect to the one used to build the training set. Some potential implications of the method for humanoid robotics are also discussed.

1 INTRODUCTION

Mathematical models of human posture control are used in the analysis of experiments as well as in the control of humanoid robots. For this reason system identification techniques have been developed for the identification of human balance as dynamic system with feedback control (van der Kooij et al., 2007; van der Kooij et al., 2005; van Asseldonk et al., 2006; Goodworth and Peterka, 2018; Mergner, 2010; Engelhart et al., 2014; Pasma et al., 2014; Jeka et al., 2010; Boonstra et al., 2014). Most of the studies performed on human posture control exploit linear models such as the *independent channel* model (Peterka, 2002), and in general assume a linear and time invariant behavior for human posture control (Engelhart et al., 2016). Linear models have the advantage of being simple to analyze and relatively easy to be fit on the data. However, experiments revealed that human posture control exhibits nonlinearities such as dead-bands and gain-non-linearity. Nonlinear models

are more complex to be fit on human data and, in the general case expensive iterative procedures should be used. In this work we propose a deep learning system to identify the parameters of a nonlinear bio-inspired posture control system, the DEC (*Disturbance Estimation and Compensation*) System. The obtained set of parameters represents a concise and expressive representation of the outcome of a posture control experiment that can be used for scientific studies and as a basis of future diagnostic tools for clinicians. The proposed technique is based on *Convolutional Neural Networks*, CNN. Such a deep learning system has been recently applied with promising result to human movement analysis, e.g. in (Abdu-Aguye and Gomaa, 2019), but so far it has not been a tool typically used in posture control analysis. The use of CNN is promising in this context because it allows to exploit local features in the time profile of the signals together with the frequency domain description of the data, as it will be clear from the description of the input features in section 2.3

---

[a] https://orcid.org/0000-0001-5520-8974

[b] https://orcid.org/0000-0001-7231-164X

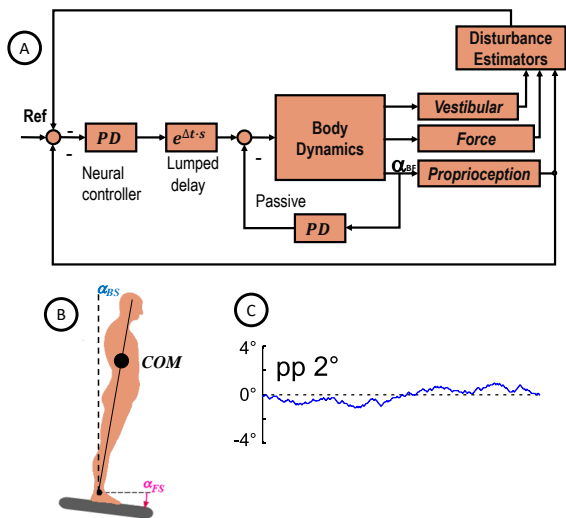[c] https://orcid.org/0000-0001-9050-279X

Figure 1: A scheme of a controller based on the DEC concept. (A) the sensory inputs are used to reconstruct the physical disturbances acting on the body. Such disturbances are compensated feeding them in the form of an *angle equivalent* as input to the servo controller. (B) The single inverted pendulum model used to simulate human posture control. The kinematics are described by the sway angle of the center of mass (COM) of the body α_{BS} and by the support surface tilt α_{FS}. (C) The *Pseudo-Random Ternary Signal*, PRTS, used as reference for the support surface tilt.

2 METHODS

2.1 Posture Control Scenario: Support Surface Tilt

The scenario considered here models a human (or humanoid) balancing on a tilting support surface. The support surface tilt α_{FS} represents the input of the system and it is the same for all the simulations. The profile of the tilt of the support surface is the *pseudo-random ternary sequence*, PRTS, shown in Fig. 1 (C). Such stimulus is used in human experiments because, thanks to its pseudo-random nature, it is not predictable for the subject (Peterka, 2002). Furthermore it is composed by a sequence of velocity steps suitable to excite the dynamics of the system over several frequencies. The output of the system is the sway of the COM α_{BS}.

2.2 Human and Humanoid Posture Control: The DEC Model

The DEC concept provides a model of the human postural control mechanisms (Mergner, 2010; Lippi and Mergner, 2017). This approach has been applied to

multiple DoF robots (Lippi and Mergner, 2017; Lippi et al., 2013; Zebenay et al., 2015; Ott et al., 2016; Lippi, 2018; Hettich et al., 2013; Hettich et al., 2015). In this work the implications of a modular control architecture will not be covered because the proposed single inverted pendulum (SIP) model consists only of one control module. A general scheme describing the DEC control is shown in Fig. 1. In general a posture control system based on the DEC concept is implemented as: (1) A servo loop, implemented as a PD controller (neural controller in Fig. 1). In the presented 1 DoF case the controlled variable consists in the body center of mass with sway with respect to the gravitational vertical passing through the ankle joint α_{BS}, where *BS* stands for *Body in Space*. (2) The disturbance estimations are, in general, identifying support surface rotation and translation, external contact forces and field forces such as gravity . The sensory channels are shown in Fig. 1 as *Vestibular*, *Proprioception*, and *Force*. The disturbance estimates are fed into the servo so that the joint torque on-line compensates for the disturbances while executing the desired movements. The *lumped delay* in Fig. 1 represents all the delay effects that in humans (but also in real world humanoids) are distributed (Antritter et al., 2014; Hettich et al., 2014). The model used in this work considers gravity and support surface tilt as disturbances. Specifically the estimators are defined as follows:
Gravity estimator

$$T_G = G_g \alpha_{BS}^{vest} \tag{1}$$

where G_g is a gain associated with the estimator. In the framework of the DEC control the disturbances are represented by an angle equivalent, i.e. the body lean that would produce, in a linear approximation, the disturbance torque as gravitational torque. This makes all the values that are summed to obtain the input of the neural controller (error and disturbances) expressed in radians. In the specific case of the gravitational torque the equivalent angle is the body lean α_{BS}^{vest}. With an ideal G_g of 1 and a proportional gain $K_p = mgh$, where m is body mass, g gravity acceleration and h is the height of the COM with respect to the ankle joint, the gravity would be exactly compensated. When fitting the model to human behavior the gravity appears to be slightly under-compensated (Hettich et al., 2014; Assländer et al., 2015). In this work G_g will be set to 1, and hence the gravity compensation gain will be determined by K_p. The signal α_{BS}^{vest} comes from the vestibular system and it is affected by a noise $\nu(N_V)$ with frequency power density N_v^2/f, where N_v is a parameter of the system.

Support surface tilt estimator

$$\alpha_{FS} = \int_0^t f_\theta \left(\frac{d}{dt}\alpha_{BS}^{vest} - \frac{d}{dt}\alpha_{BF}^{prop} \right) \qquad (2)$$

where α_{BF}^{prop} is the ankle joint angle signal from proprioception. *BF* stands for *Body-to-Foot*, *FS* stands for *Foot-in-Space*. In some implementations of the DEC concept the integral in eq. 2 is implemented as a leaky integrator (Lippi and Mergner, 2017), in this work it is set to zero at the beginning of the simulation. The function f_θ is a dead-band threshold defined as

$$f_\theta(\alpha) = \begin{cases} \alpha + \theta & if & \alpha < -\theta \\ 0 & if & -\theta < \alpha < \theta \\ \alpha - \theta & if & \alpha > \theta \end{cases} \qquad (3)$$

The threshold function is added to reproduce the behavior observed in humans (Mergner et al., 2009; Mergner et al., 2003). The reconstructed body-in-space variable used for the servo controller is then

$$\alpha_{BS}^{servo} = \alpha_{FS} - \alpha_{BF}^{prop} \qquad (4)$$

affected by the non-linearity introduced by f_θ. Considering that in the present scenario the simulated agent aims to maintain the upright stance, i.e. the reference signal is zero, the total torque commanded by the servo controller is:

$$\tau_{active} = -e^{-s\Delta}(K_p + sK_d)\left(T_g + \alpha_{BS}^{servo}\right) \qquad (5)$$

where K_d is the derivative coefficient for the PD controller (for the sake of brevity in this equation and the following the derivatives, the integrators and the delay are represented using Laplace transform variable s so that they can be conveniently expressed as a multiplicative operator, although the rest of the formula refers to operations in time domain). Δ is the lump delay. Notice that the derivative component is acting also on gravity compensation, representing a sort of anticipation of the disturbance. There is also a passive torque acting on the ankle joint defined as:

$$\tau_{passive} = -(K_p^{pass} + sK_d^{pass})\left(\alpha_{BF}^{prop}\right) \qquad (6)$$

In order to show the role of all the parameters (listed in Table 1, here highlighted in blue) the total torque can be written as:

$$\tau_{ankle} = \tau_{active} + \tau_{passive}$$

$$= -e^{-s\Delta}(K_p + sK_d)$$

$$\left(\alpha_{BS}^{vest} + \alpha_{FS} - \frac{1}{s}f_\theta\left(s(\alpha_{BS}^{vest} + \nu(N_v)) + s\alpha_{BF}^{prop}\right)\right)$$

$$-(K_p^{pass} + sK_d^{pass})\left(\alpha_{BF}^{prop}\right) \qquad (7)$$

2.3 The Training Set

The training and the validation set for the neural network have been generated with random parameters from uniform distributions (the range is shown in Table. 1). A set of parameters is used as a sample only if the behavior it produces is stable: simulations with α_{BS} amplitude larger than $5°$ are not considered realistic balancing scenarios and are discarded. Most of the stable simulations obtained with such random sampling were associated with a relatively small COM sway, the amplitude distribution is shown in Fig. 2 in blue. In order to obtain a data-set including larger oscillations, representative of a *relaxed* human behavior, the data-set was enriched with samples that were produced repeating the simulations with larger outputs ($> 0.05rad$) with parameters subject to a relatively small modification ($\approx 10\%$ of the range). The resulting enriched data-set is shown in Fig. 2 in orange. The performance of the neural network on the two sets was almost the same and hence only the enriched data-set is considered. The distribution of a realistic human data-set is discussed more in detail in section 4. The resulting data-set included 12766 samples. Half of the samples are used for training, the other half divided equally between *validation set* and *test set*.

The neural network is trained to identify the simulation parameters on the basis of body sway profiles. The *Target* for the training is represented by the vector of parameters, centered with respect to the mean normalized by the standard deviation (both computed on the training set). The *Input* is a convenient representation of the output. The simulation was performed with a fixed integration step of 1 *ms* and produced 12100 α_{BS} samples with a resolution of 10 *ms*. In order to adapt the signal to the convolutional network used the input was transformed into a two channel image, with the channels representing, respectively, the modulus and the phase of the FFT of the signal computed on non overlapping time windows. Empirical tests have shown that the best performance was achieved with a time window of 110 samples resulting in a square 110×110 two-channel image (Fig. 3 above).
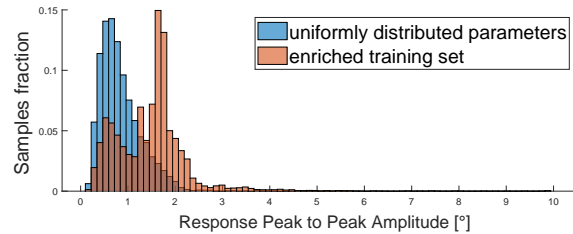

Figure 2: Peak-to-peak body sway amplitude distribution.

Table 1: Simulation parameters with an overview of their distributions in the examples used as training and validation set. *min* and *max* represent the minimum and the maximum values of the uniform distributions used to generate the samples. *Mean* and *std* (standard deviation) are computed on the selected simulations that resulted in a stable behavior (i.e. maximum α_{BS} oscillation under $5°$) and included the *enrichment* (see text).

| Parameter	Symbol	min	max	mean	std	unit
Active proportional gain	K_p	503.3943	1258.4857	811.2951	338.0956	$\frac{N \cdot m}{rad}$
Active derivative gain	K_d	125.8486	377.5457	284.5640	122.7999	$\frac{N \cdot m \cdot s}{rad}$
Passive stiffness	$K_{p_{pass}}$	62.9243	377.5457	312.2075	102.1054	$\frac{N \cdot m}{rad}$
Passive damping	$K_{d_{pass}}$	62.9243	188.7729	174.3144	68.5447	$\frac{N \cdot m \cdot s}{rad}$
Vestibular noise gain	N_V	0	1.0000	0.4695	0.2928	1
Foot rotation velocity threshold	θ_{vfs}	0	0.0052	0.0003	0.0124	rad/s
Lumped delay	Δ	0	0.2400	0.1210	0.0672	s
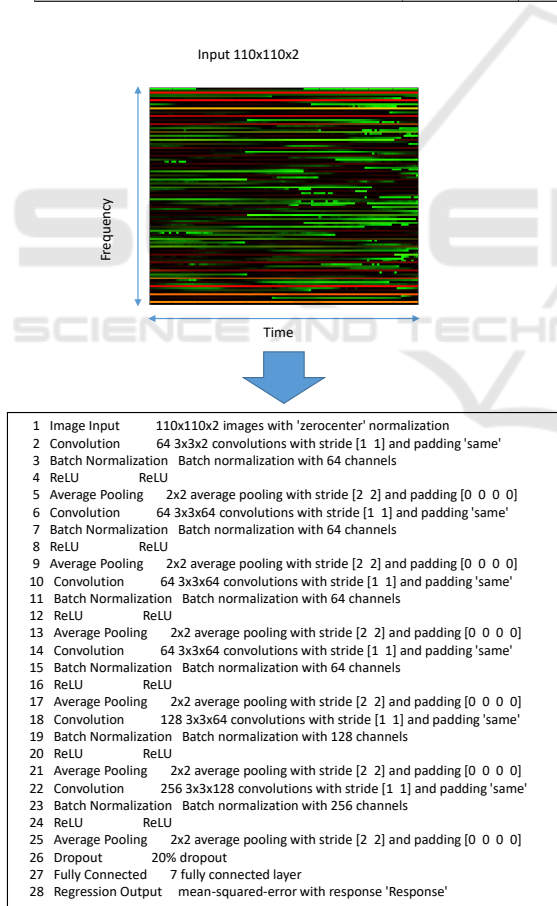
Figure 3: (Top) Example of the appearance of an input sample. The image has two channels, red and green, associated to the modulus the phase of the FFT of the body sway over a time window, respectively. (Bottom) Neural network architecture.

2.4 The Neural Network

The neural network architecture is shown in Fig 3, where the layers are listed. The structure of the network with its hyperparameters was tuned on the basis of the performance on the validation set. The network has been implemented with Deep Learning Toolbox[TM]. Such network is not designed for 1-D convolution and hence the input is transformed into an image. The filters of convolutional layers apply the same weight to different parts of the input. The axis of the input image can be seen as *time* and *frequency*. This means that the convolutional filters allow the network to recognize pattern translated in time (horizontal) and in frequency (vertical). While the former invariance has the understandable meaning that the network is able to recognize the same movement patterns appearing at different times, as expected from 1-D CNN applied to time series, the latter has no straightforward physical explanation. An example of the activation of the filters in the first layers is shown in Fig. 4. The network has been trained using *stochastic gradient descent with momentum* as policy. The training was set to a limit of 100 epochs. The data-set is divided in three subsets: 6383 samples used as *training set*, 3192 as *validation set*, and 3191 as *test set* respectively. The loss function is the *Mean Squared Error* MSE, coherently for the regression task. The evolution of the MSE through the training iterations is shown in Fig. 5.
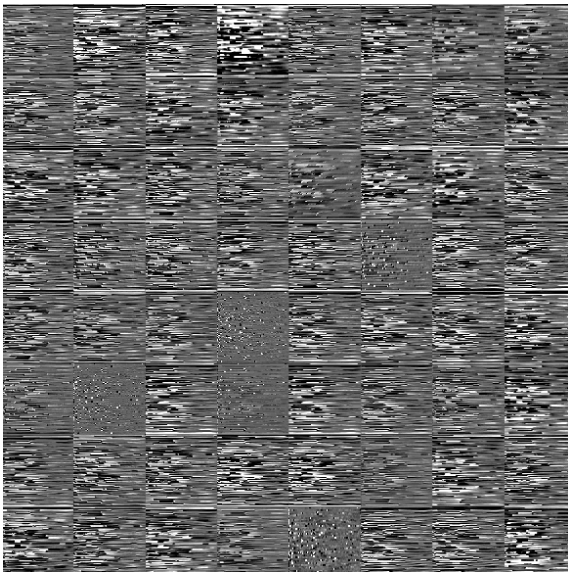
Figure 4: Graphic rendering of the first convolutional layer of the network. Each image in the 8×8 grid represent the response of one of the 64 filters to the input image. Lighter pixels are associate with a larger activation than darker pixels.
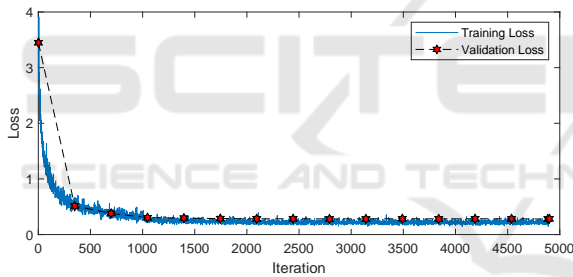

Figure 5: Training and validation loss through the iterations.

3 RESULTS

3.1 Validation Set and Test Set

The loss function used for the training was half the MSE. The *loss* on the *validation set* is 0.2851, the *loss* on the *test set* is 0.2775. They are comparable to the *loss* obtained for the training set which is 0.2250. Figure 5 shows how the loss function is stable for several iteration on both training set and validation set. Thanks to the availability of a large enough number of samples the system is not showing signs of large over-fitting. This was reflected by the fact that there was no early stop due to validation error. An example of the output obtained using a specific sample is shown in Fig. 6.
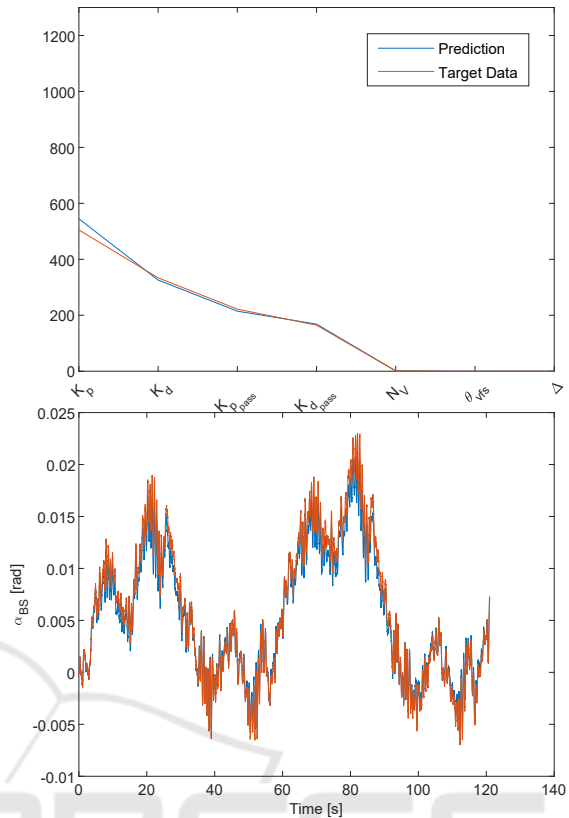

Figure 6: The CNN applied to a specific sample: (Top) network output and target sample, and (Bottom) the associated α_{BS}.

3.2 Double Inverted Pendulum Case

The system is now applied to DIP data produced with a simulation with default parameters (Hettich et al., 2013). In Fig. 7 the control parameters for the ankle module used in the simulation are compared with the ones identified by the CNN. The accuracy of the result is, as expected slightly worse than the one obtained using the validation set. with a SE (Squared Error) for the normalized parameters of 10.4783, as compared to the smaller validation set MSE of 0.5702.

3.3 Identification of Human Posture Control Parameters

The CNN is here applied to human data. A single trial from one subject is used. Like in the previous example, the experiment does not include any device to block the hip so that the center of mass sway is influenced by the ankle-hip coordination. The identified parameters and the simulated body sway are shown in Fig. 8. The peak-to-peak sway amplitude exhibited by the human subject was $2.8533°$. This exam-
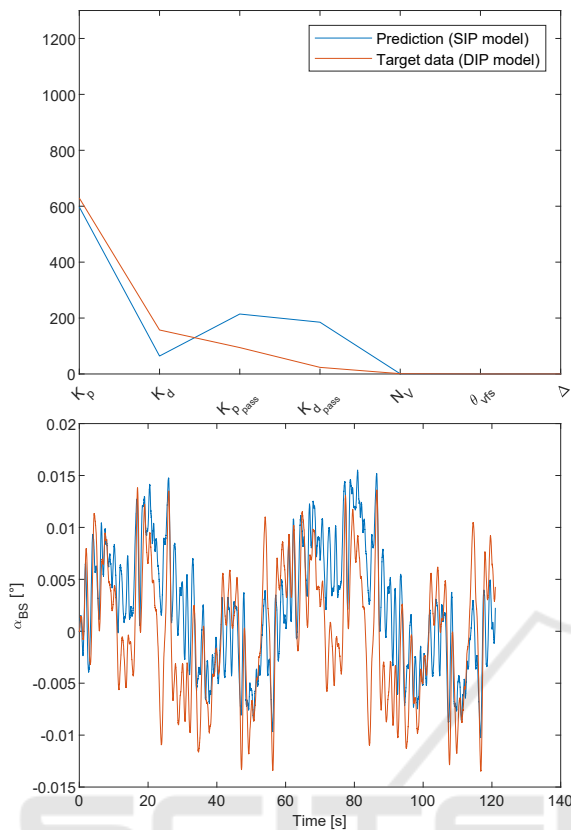
Figure 7: The CNN applied to a sample produced with a double inverted pendulum (DIP) model: (Top) network output compared with the parameters applied to the control of the ankle in the DIP model. The hip has also its set of parameters, not displayed. In (Bottom) the α_{BS} trajectory produced by the DIP is compared with the one of a SIP using the parameters predicted by the CNN.

ple suggests that it is beneficial to include larger body sway examples in the training-set. The result in Fig. 8 shows a good, although not perfect, similarity between the simulation and the original data.

4 CONCLUSIONS AND FUTURE WORK

In this work we presented a method for posture control parameter identification based on CNN. The system provides an efficient way to fit a model of the non-linear bio-inspired control system DEC on experimental data. This represents an advantage with respect to previous solutions relying on iterative methods. With the used training set noisy by design and because noise power is one of the parameters, the system provides an average error that is non-zero. The obtained parameters can be used as a description of
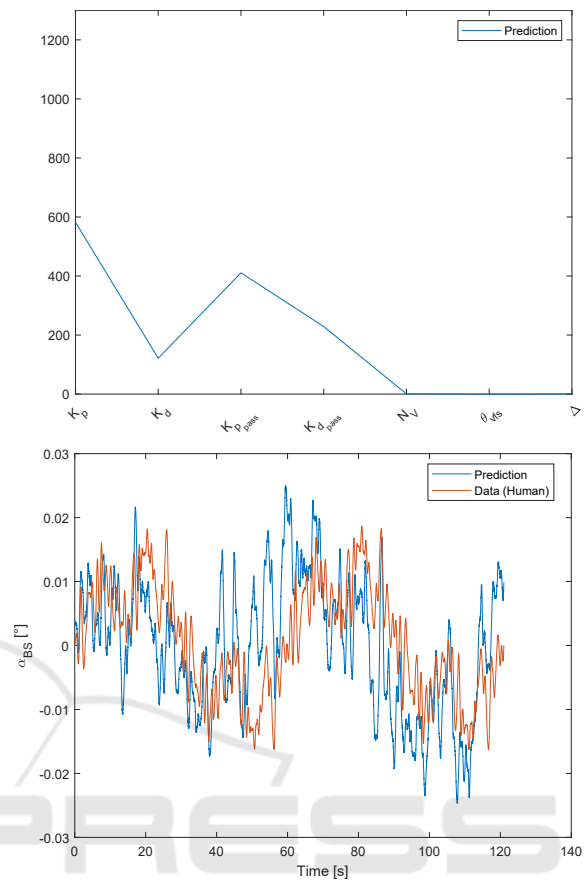

Figure 8: The CNN applied to data from a human experiment. (Top) The identified parameters are shown. (Bottom) The original input is compared with the input produced by the simulation using the parameters identified by the CNN.

the analyzed data, as guideline for more accurate fitting procedures and as features for further analysis algorithms, for example a diagnostic tool could be implemented using SVM trained with the parameters vector as input. In general the envisaged application of the presented approach is to provide a way to integrate non-linear posture control models in diagnostics tools and decision supporting tools for clinicians(Exarchos et al., 2015; Rammazzo et al., 2016).

The training set is produced with parameters from uniform distributions, filtered with the constraint, checked empirically, so that they produce a stable simulation. In order to obtain more *human-like* examples the data-set has been enriched with samples producing larger body sways. Future work may introduce preliminary studies on the distribution of human data, generating some training samples from samples obtained by fitting the model on the experimental data. The CNN can also be tested *a posteriori* comparing the distribution of the parameters it produces on the validation set with the expected distribution on

real data. This can help the process of choosing between different possible network hyperparameter sets as shown in (Sforza et al., 2011; Sforza and Lippi, 2013).

The SIP model used in this work proved to be suitable to describe the analyzed posture control scenario, this even in the sub-optimal case of identifying the control parameter of the ankle joint in a DIP model. Future work will aim to the design of a solution that identifies also the parameters controlling the hip joint, which is known to have a relevant function in balancing (Hettich et al., 2014; Horak and Nashner, 1986; Park et al., 2004).

The modeling and the analysis of human posture control and balance provides and get inspirations from the study of humanoid robots control, e.g. (Choi and Kim, 2007; Abedi and Shoushtari, 2012; Zebenay et al., 2015; Mergner and Lippi, 2018), or can be used to improve the design of assistive systems and devices (Chugo et al., 2019; Mergner and Lippi, 2019). The proposed deep-learning-based tool will be also published as a tool to benchmark humanoids and wearable devices (Torricelli et al., 2020), within the framework of the COMTEST project (Lippi et al., 2019) that aims to make a posture control testbed available for the humanoid robotics community.

ACKNOWLEDGEMENTS

REFERENCES

Abdu-Aguye, M. G. and Gomaa, W. (2019). On the feasibility of on-body roaming models in human activity recognition. In *Proceedings of the 16th International Conference on Informatics in Control, Automation and Robotics - Volume 1: ICINCO,*, pages 507–516. INSTICC, SciTePress.

Abedi, P. and Shoushtari, A. L. (2012). Modelling and simulation of human-like movements for humanoid robots. In *Proceedings of the 9th International Conference on Informatics in Control, Automation and Robotics - Volume 1: ICINCO,*, pages 342–346. INSTICC, SciTePress.

Antritter, F., Scholz, F., Hettich, G., and Mergner, T. (2014). Stability analysis of human stance control from the

system theoretic point of view. In *Control Conference (ECC), 2014 European*, pages 1849–1855. IEEE.

Assländer, L., Hettich, G., and Mergner, T. (2015). Visual contribution to human standing balance during support surface tilts. *Human movement science*, 41:147–164.

Boonstra, T. A., van Vugt, J. P., van der Kooij, H., and Bloem, B. R. (2014). Balance asymmetry in parkinson's disease and its contribution to freezing of gait. *PLoS One*, 9(7):e102493.

Choi, Y. and Kim, D. (2007). On the balancing control of humanoid robot. In *Proceedings of the Fourth International Conference on Informatics in Control, Automation and Robotics - Volume 2: ICINCO,*, pages 248–252. INSTICC, SciTePress.

Chugo, D., Koyama, M., Yokota, M., Kawazoe, S., Muramatsu, S., Yokota, S., Hashimoto, H., Katayama, T., Mizuta, Y., and Koujina, A. (2019). Sitting Assistance that Considers User Posture Tolerance. In *Proceedings of the 16th International Conference on Informatics in Control, Automation and Robotics - Volume 2: ICINCO,*, pages 489–496. INSTICC, SciTePress.

Engelhart, D., Boonstra, T. A., Aarts, R. G., Schouten, A. C., and van der Kooij, H. (2016). Comparison of closed-loop system identification techniques to quantify multi-joint human balance control. *Annual Reviews in Control*, 41:58–70.

Engelhart, D., Pasma, J. H., Schouten, A. C., Meskers, C. G., Maier, A. B., Mergner, T., and van der Kooij, H. (2014). Impaired standing balance in elderly: a new engineering method helps to unravel causes and effects. *Journal of the American Medical Directors Association*, 15(3):227–e1.

Exarchos, T. P., Bellos, C., Bakola, I., Kikidis, D., Bibas, A., Koutsouris, D., and Fotiadis, D. I. (2015). Management and modeling of balance disorders using decision support systems: the embalance project. In *GeNeDis 2014*, pages 61–67. Springer.

Goodworth, A. D. and Peterka, R. J. (2018). Identifying mechanisms of stance control: a single stimulus multiple output model-fit approach. *Journal of neuroscience methods*, 296:44–56.

Hettich, G., Assländer, L., Gollhofer, A., and Mergner, T. (2014). Human hip—ankle coordination emerging from multisensory feedback control. *Human Movement Science*, 37:123–146.

Hettich, G., Lippi, V., and Mergner, T. (2013). Human-like Sensor Fusion Mechanisms in a Postural Control Robot. In Londral, A. E., Encarnacao, P., and Pons, J. L., editors, *Proceedings of the International Congress on Neurotechnology, Electronics and Informatics. Vilamoura, Portugal*, pages 152–160.

Hettich, G., Lippi, V., and Mergner, T. (2015). Human-like sensor fusion implemented in the posture control of a bipedal robot. In *Neurotechnology, Electronics, and Informatics*, pages 29–45. Springer.

Horak, F. B. and Nashner, L. M. (1986). Central programming of postural movements: adaptation to altered support-surface configurations. *Journal of neurophysiology*, 55(6):1369–1381.

Jeka, J. J., Allison, L. K., and Kiemel, T. (2010). The dynamics of visual reweighting in healthy and fall-prone older adults. *Journal of Motor Behavior*, 42(4):197–208.

Lippi, V. (2018). Prediction in the context of a human-inspired posture control model. *Robotics and Autonomous Systems*.

Lippi, V. and Mergner, T. (2017). Human-derived disturbance estimation and compensation (dec) method lends itself to a modular sensorimotor control in a humanoid robot. *Frontiers in neurorobotics*, 11:49.

Lippi, V., Mergner, T., and Hettich, G. (2013). A bio-inspired modular system for humanoid posture control. *In: Ugur, E., Oztop, E., Morimoto, J., and Ishii, S. (Eds) Proceedings of IROS 2013 Workshop on Neuroscience and Robotics "Towards a robot-enabled, neuroscience-guided healthy society"*.

Lippi, V., Mergner, T., Seel, T., and Maurer, C. (2019). COMTEST project: A complete modular test stand for human and humanoid posture control and balance. In *2019 IEEE-RAS 19th International Conference on Humanoid Robots (Humanoids) Toronto, Canada. October 15-17*.

Mergner, T. (2010). A neurological view on reactive human stance control. *Annual Reviews in Control*, 34(2):77–198.

Mergner, T. and Lippi, V. (2018). Posture control–human-inspired approaches for humanoid robot benchmarking: Conceptualizing tests, protocols and analyses. *Frontiers in Neurorobotics*, 12:21.

Mergner, T. and Lippi, V. (2019). Integrating posture control in assistive robotic devices to support standing balance. In Carrozza M., Micera S., P. J., editor, *Wearable Robotics: Challenges and Trends. WeRob 2018.*, volume 22 of *Biosystems & Biorobotics*. Springer, Cham.

Mergner, T., Maurer, C., and Peterka, R. J. (2003). A multisensory posture control model of human upright stance. *Progress in Brain Research*, 142:189–201.

Mergner, T., Schweigart, G., and Fennell, L. (2009). Vestibular humanoid postural control. *Journal of Physiology - Paris*, 103:178–194.

Ott, C., Henze, B., Hettich, G., Seyde, T. N., Roa, M. A., Lippi, V., and Mergner, T. (2016). Good posture, good balance: Comparison of bioinspired and model-based approaches for posture control of humanoid robotsg. *IEEE Robotics & Automation Magazine*, 23(1):22–33.

Park, S., Horak, F. B., and Kuo, A. D. (2004). Postural feedback responses scale with biomechanical constraints in human standing. *Experimental brain research*, 154(4):417–427.

Pasma, J., Engelhart, D., Schouten, A., Van der Kooij, H., Maier, A., and Meskers, C. (2014). Impaired standing balance: the clinical need for closing the loop. *Neuroscience*, 267:157–165.

Peterka, R. (2002). Sensorimotor integration in human postural control. *Journal of Neurophysiology*, 88(3):1097–1118.

Rammazzo, L., Kikidis, D., Anwer, A., Macdonald, N., Kyrodimos, E., Maurer, C., Wuyts, F., Luxon, L.,

Bibas, A., and Bamiou, D.-E. (2016). Embalance-validation of a decision support system in the early diagnostic evaluation and management plan formulation of balance disorders in primary care: study protocol of a feasibility randomised controlled trial. *Trials*, 17(1):435.

Sforza, F. and Lippi, V. (2013). Support vector machine classification on a biased training set: Multi-jet background rejection at hadron colliders. *Nuclear Instruments and Methods in Physics Research Section A: Accelerators, Spectrometers, Detectors and Associated Equipment*, 722:11–19.

Sforza, F., Lippi, V., and Chiarelli, G. (2011). Rejection of multi-jet background in pp→ ev+ jj channel through a svm classifier. In *Journal of Physics: Conference Series*, volume 331, pages 32–45. IOP Publishing.

Torricelli, D., Mizanoor, R. S., Lippi, V., Weckx, M., Mathijssen, G., Vanderborght, B., Mergner, T., Lefeber, D., and Pons, J. L. (2020). Benchmarking human likeness of bipedal robot locomotion: State of the art and future trends. In *Metrics of Sensory Motor Coordination and Integration in Robots and Animals*, pages 147–166. Springer.

van Asseldonk, E. H., Buurke, J. H., Bloem, B. R., Renzenbrink, G. J., Nene, A. V., van der Helm, F. C., and van der Kooij, H. (2006). Disentangling the contribution of the paretic and non-paretic ankle to balance control in stroke patients. *Experimental neurology*, 201(2):441–451.

van der Kooij, H., van Asseldonk, E., and van der Helm, F. C. (2005). Comparison of different methods to identify and quantify balance control. *Journal of Neuroscience Methods*, 145(1-2):175–203.

van der Kooij, H., van Asseldonk, E. H. F., Geelen, J., van Vugt, J. P. P., and Bloem, B. R. (2007). Detecting asymmetries in balance control with system identification: first experimental results from parkinson patients. *Journal of Neural Transmission*, 114(10):1333.

Zebenay, M., Lippi, V., and Mergener, T. (2015). Human-like humanoid robot posture control. In *2015 12th International Conference on Informatics in Control, Automation and Robotics (ICINCO)*, volume 2, pages 304–309. INSTICC, SciTePress.